

Modulation of the Physical Properties of Lead Zirconate by the Stress-Induced Structural Defects

Marina Sirota, Kamaludin Abdulvakhidov, Tatiana Lastovina, Anna Pnevskaya, Elza Ubushaeva, Pavel Plyaka, Alexander Nazarenko, Marina Vitchenko, Irina Mardasova, and Andriy Budnyk*

The influence of the stress-induced structural defects in PbZrO_3 on its structural, optical, and dielectric properties is studied systematically for the first time. The PbZrO_3 ceramics is prepared by a conventional solid state synthesis. The structural defects in PbZrO_3 are generated by the combined action of mechanical compression due to applied pressure in the 40–320 MPa range and the shear strain appearing in the rotating Bridgman anvils. The pressure dependencies of the cell parameters, the mean size of coherent scattering regions and the microstrain, the Debye characteristic temperature, and the isotropic Debye–Waller factor are calculated from processing the X-ray diffraction (XRD) data and commented on. The local structure around Pb and Zr atoms is probed with the X-ray absorption near edge structure (XANES). This approach demonstrates the possibility of controlling the dielectric, electronic, and structural parameters of PbZrO_3 by changing the concentration of the stress-induced structural defects.

1. Introduction

Lead zirconate (PZO) is a model antiferroelectric (AFE) compound with perovskite structure.^[1] Its properties were theoretically predicted by Kittel and described experimentally by Shirane and Sawaguchi in the 1950s.^[2] The performance of PZ-based AFE materials can be improved by tailoring the phase transformation behavior, which is mainly determined by the constitutions and the external field.^[3] Perovskite structure-based oxides are multifunctional materials with relevance in heterogeneous catalysis and surface chemistry, and play a vital role in the

field of energy conversion and storage.^[4] For instance, lead zirconate titanate (PZT) solid solutions are widely utilized for the fabrication of electromechanical, electronic, and electrooptical devices.^[5] PZO has recently received renewed attention as a potential candidate material for high-energy-density dielectric capacitors.^[6]

At room temperature PZO demonstrates the orthorhombic centrosymmetric space group $Pbam$.^[7] A characteristic dielectric anomaly occurs at $\approx 233^\circ\text{C}$, which is right below the Curie temperature ($T_c = 236^\circ\text{C}$).^[1] It signalizes the first-order-like phase transition from the AFE to paraelectric (PE) phase through a ferroelectric (FE) state.^[2] The exact temperature of transition depends on the particularities of each system, such as the purity,

crystallinity, and defectivity. The PZO dielectric constant maxima at rising and falling temperatures are different by $\approx 4^\circ$ due to a phase transformation.^[8] The AFE-PE phase transition was reportedly observed in the temperature interval of 212–228 $^\circ\text{C}$, while the FE-PE phase was recognized in the range of 232–236 $^\circ\text{C}$. It was recently shown that the AFE state is a manifestation of an incommensurate phase, and the AFE to PE transition is driven by the softening of a single lattice mode via flexoelectric coupling.^[9] Later, a nonmodulated phase existing between the cubic and the incommensurate phases was found under application of hydrostatic pressure, demonstrating that PZO is not a single-instability-driven system.^[10]


An intermediate or transient phase of PZO appears in the region between the high-temperature cubic state and the low-temperature AFE state, where the FE domains occur and coexist with the AFE domains.^[11] Although being commonly ascribed to the presence of various admixtures or defects in the crystal lattice, the true nature of the weak FE behavior is yet to be revealed.^[12] The original explanation of the FE phase by the presence of impurities was later dismissed by experimental evidence of its disappearance when calcium and lanthanum were purposefully introduced.^[13] Alternatively, it was ascribed to structural defects such as Pb vacancies in a study on PZO modified with Nb_2O_5 .^[14] Such a cation deficiency in the Pb sublattice occurs under the high-temperature growth of PZO single crystals or due to prolonged exposure to high temperatures, and expands the existence intervals of either the AFE-FE transition or the FE phase.^[15]

Dr. M. Sirota, Dr. M. Vitchenko, Dr. I. Mardasova
Don State Technical University
Gagarin Sq. 1, Rostov-on-Don 344000, Russia

Prof. K. Abdulvakhidov, A. Pnevskaya
Southern Federal University
Bolshaya Sadovaya Str. 105/42, Rostov-on-Don 344090, Russia

Dr. T. Lastovina, Dr. P. Plyaka, Dr. A. Nazarenko, Dr. A. Budnyk
Southern Scientific Centre of the Russian Academy of Sciences
Chehova Str. 41, Rostov-on-Don 344006, Russia
E-mail: budnik@ssc-ras.ru

Dr. E. Ubushaeva
Moscow Aviation Institute
Volokolamskoe shosse, 4, Moscow 125993, Russia

 The ORCID identification number(s) for the author(s) of this article can be found under <https://doi.org/10.1002/pssa.202000782>.

DOI: 10.1002/pssa.202000782

In a recent study on PZO ceramics, Liu has indicated that neither defects nor impurities are behind the intermediate phase in PZO.^[16] In that work, the PZO powders were calcined at 900 °C for 4 h, and then the pressed PZO pellets were sintered at 1200–1250 °C for 3–4 h. The dielectric permittivity measurements demonstrated that the intermediate phase may or may not appear on cooling before the AFE phase transition, regardless of the sintering conditions. Furthermore, the intermediate phase has emerged only in specimens with a low content of pseudocubic [001]_c domains, which are known to stabilize the AFE phase by suppressing the effect of out-of-phase oxygen octahedral rotation.

An experimental inquiry into the domain structure formation at the PE to AFE phase transition in PZO crystals was performed by polarization microscopy and diffractometry on two groups of samples grown at 1040 °C for 4 h and 1050 °C for 20 h, respectively.^[17] Thermo-optical examination of the first group found a single phase transition (PE to AFE) with a boundary corresponding to (310) planes. This was explained by the presence of planar defects in the form of crystallographic shear planes.^[18] In the second group, an intermediate rhombohedral FE phase was observed. While passing from both the AFE orthorhombic phase to the FE phase and from the FE to PE cubic phase, optically observed interfaces did not demonstrate determined crystallographic orientation or a regular structure due to structural non-homogeneity, as revealed by X-ray examination.^[17]

The structural defects, regardless of their origin and type, affect phase transitions in PZO.^[19] In particular, they can initiate an intermediate FE phase transition or suppress it. Therefore, one may tune the physical properties of PZO by purposely varying the concentration and type of defects. Such defects can be introduced by processing the PZO powder in the Bridgman anvils, allowing for high-pressure torsion. That is a twofold treatment, which includes mechanical activation (or simply mechanoactivation) and subsequent consolidation of the powder.

We have studied the effect of structural defects (dislocations and point defects) on the physical properties of $\text{PbZr}_{0.58}\text{Ti}_{0.42}\text{O}_3$,^[20] $\text{PbZr}_{0.56}\text{Ti}_{0.44}\text{O}_3$,^[21] and PbTiO_3 ^[22] as well as several relaxor ferroelectrics.^[23] In the studied systems, the nonideal crystal lattice not only leads to an additional attenuation of the intensity of the Bragg maxima due to static displacements, but also modifies the expression for the Debye–Waller attenuation factor, B .^[24] It is also known that both the particle size and structural defects affect the vibrational spectrum and the characteristic Debye temperature of solids, Θ_D .^[25] While B characterizes the influence of temperature on the attenuation of Bragg reflections by the crystal lattice, the second parameter, Θ_D , defines the strength of interatomic bonds.

Therefore, it is of practical importance to examine how the properties of PZO respond to mechanical activation. In this work, the previously developed methodology^[20–22] is utilized to assess the impact of the stress-induced structural defects on phase transitions, structural parameters, electrophysical properties, and lattice dynamics of PZO ceramics.

2. Results and Discussion

The X-ray diffraction (XRD) spectra of mechanoactivated samples preserved the diffraction pattern of the pristine PbZrO_3 powder, as shown in Figure 1 for PZO and PZO160. Although the

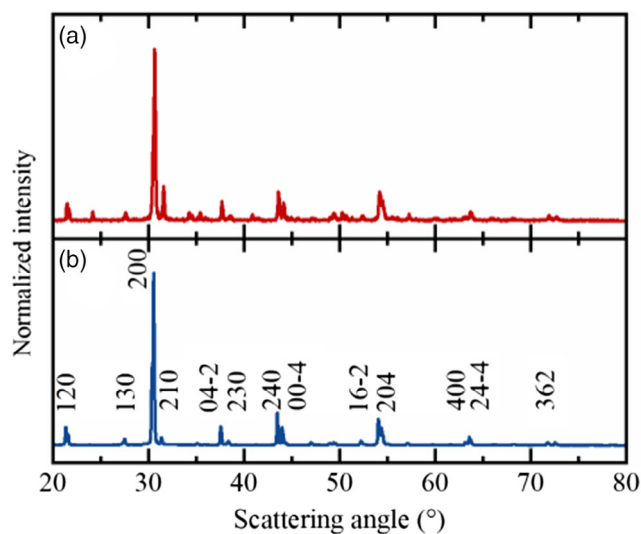


Figure 1. a) XRD patterns of PZO160 and b) PZO powders.

measured spectra had increased noise at lower Bragg angles, which was attributed to the partial amorphization of the crystallite phase under mechanical stress. Rietveld refinement was performed to identify the space group and the impact of mechanical activation on crystallographic unit cell parameters. The $Pbam$ space group is recognized in all the samples; the corresponding reflections are indicated above the PZO pattern in Figure 1b. Impurity phases were not detected. The centrosymmetric $Pbam$ structure is often considered to describe the PZO symmetry at room temperature.^[2c,26] The antiparallel displacements of cations in the (110) planes and the oxygen octahedral tilt in the system $a^-a^-c^0$ of Glazer are counted to be immanent for the structure.^[27] The highly anharmonic Pb hopping reportedly contributes to the existence of polar clusters in the PE cubic phase of PZO.^[28]

The results of Rietveld refinement allowed us to plot the pressure dependencies of the unit cell parameters (a , b , and c). As shown in Figure 2a, the parameters change uniformly with increasing pressure in a damped-oscillation manner. They have fallen after initial loadings and just moderately decreased at pressures of 120 and 160 MPa. The response pattern is repeated for the pressures over 160 MPa, although with a lower magnitude.

For deeper inquiry into the structural perfection of crystallites and to estimate the density of dislocations, ρ_D , in mechanically activated samples, the mean size of coherent scattering regions, D , and the microstrain, $\Delta d/d$, both contributing to the broadening of diffraction peaks, were evaluated using a classical approximation method.^[29] The obtained values are displayed in Figure 2b as pressure dependencies.

The pressure of 40 MPa causes a double reduction of the mean size of the coherent scattering regions, which then slowly and only partially recovered toward 280 MPa, most probably due to the intensification of diffusion and recrystallization processes. The same pressure induces the increase of the microstrain, whose behavior resembles the lattice parameter dependencies (Figure 2a), reaching maxima at 80 and 280 MPa. Because the impact of stress-generated screw dislocations on the broadening

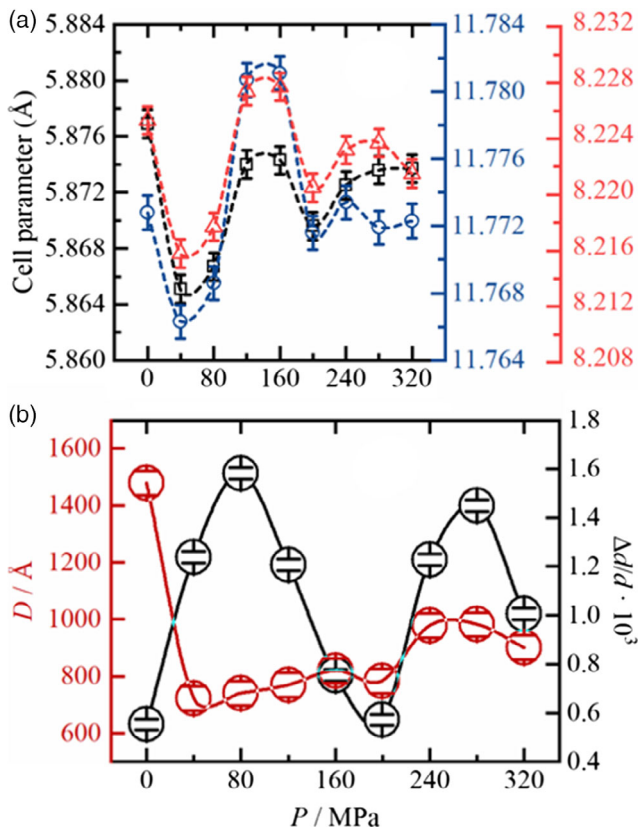


Figure 2. Pressure dependencies of PZO parameters: a) the unit cell parameters a , b , and c (black-, blue-, and red-colored scatters and ordinate axes, respectively) and b) the mean size of coherent scattering regions (red circles, left ordinate axis) and microstrain (black circles, right ordinate axis).

of XRD profiles is practically insignificant, we can assume we are dealing mainly with the edge dislocations. Supposing their chaotic distribution, we may calculate ρ_D (see Equation (S1), Supporting Information). It has the highest value at 40 MPa (Table 1), and such a pressure can be considered as a threshold, where the concentration of generated dislocations stops growing, and the point defects begin to dominate.

Thus, the structural parameters of PZO exhibit a nonmonotonic pressure dependency (Figure 2), implying that all mechanically activated powders were in different metastable states before the final sintering (at 1150 °C). This observation complies well with the earlier findings for PbTiO_3 .^[22]

The parameter ζ , which is proportional to the shear strain, was determined to be ≈ 12 by using the formula $\zeta = \ln(\frac{v}{v_0})$, where v is

the angle of rotation, r is the radius of the anvil, and d is the sample thickness.

Next, we consider how mechanical activation affects the dynamic properties of the PZO crystal lattice. According to the Debye approximation, a cubic crystal behaves as an isotropic solid where all waves of a given type propagate at the same velocity independently of their wavelength and direction. The Debye temperature of each sample was determined by the two-temperature method^[30] from the intensity ratio of diffractograms measured at 573 and 673 K (see Equation (S2), Supporting Information; raw data are not reported for brevity). The obtained values are plotted in Figure 3a as a pressure-dependent function. The Debye temperature of PZO at 673 K increases ≈ 3.6 times from its initial value at 40 MPa, and that of PZO at 573 K increases 2.6 times at 160 MPa. The former peak corresponds to the situation of maximum ρ_D and minimum D , and the latter one correlates with a rather sharp decrease of ρ_D (Table 1) and recovery (expansion) of the unit cell parameters (Figure 2b). In our study on $\text{Pb}(\text{Zr}_{0.56}\text{Ti}_{0.44})\text{O}_3$,^[21] an increase of the mean size

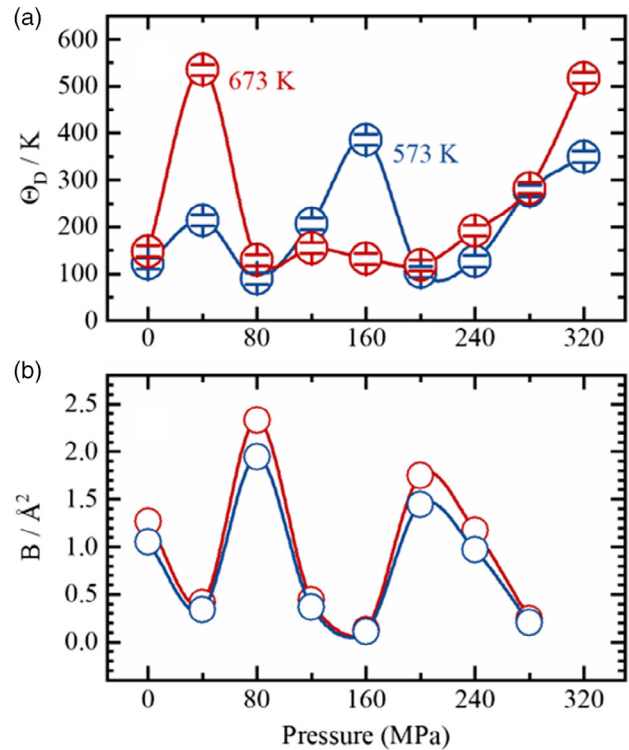


Figure 3. Pressure dependencies of the Debye temperature and the isotropic Debye–Waller factor.

Table 1. The calculated values of the density of dislocations, ρ_D , the bandgap, E_g , and the local energy levels, E_i , for PZO samples.

P [MPa]	0	40	80	120	160	200	240	280	320
Label	PZO	PZO40	PZO80	PZO120	PZO160	PZO200	PZO240	PZO280	PZO320
$\rho_D \cdot (10^8)$ [cm^{-2}]	1.26	6.88	6.85	5.8	5.0	5.1	3.3	3.3	3.2
E_g [eV]	3.556	3.419	3.374	3.577	3.4	3.571	3.419	3.549	3.556
E_i [eV]		3.11	3.09	3.071	2.759	3.062	3.184	3.184	2.963

of coherent scattering regions peaking at 160 MPa was observed during the high-temperature measurements and ascribed to the intensification of diffusion processes. This might be the case for PZO as well, although such processes are difficult to control in metastable systems.

The obtained Θ_D values were used to calculate the Debye–Waller factor, B (see Equation (S3), Supporting Information). As shown in Figure 3b, the B values for two temperatures (573 and 673 K) demonstrate a common oscillating trend with two discrepancies at 80 and 200 MPa, attributed to the lattice vibration anharmonicity. It should also be noted that although the B values of the pristine materials are equal, the highest B values for the mechanically activated PZO are twice lower than those reached earlier for the similarly treated PbTiO_3 .^[22]

The micrographs of PZO (Figure 4a) and PZO160 (Figure 4b) demonstrate that samples consist of micrometer-sized irregular grains. PZO160 also contains smaller particles covering the grains. This observation is supported by the particle size distribution histograms in Figure 3, which were built from the graphical analysis of SEM images. The histogram for PZO has a distinct maximum at 1.6 μm , whereas that for PZO160 demonstrates a strong increment in the number of particles below 1 μm and a decrement of intensity at 1.6 μm . The smaller particles were formed at the expense of larger ones. The size ratio of larger to smaller particles is ≈ 2.5 , which is of comparable magnitude to the reduction of the mean size of coherent scattering regions (Figure 2b). It is highly likely that particles (grains) would crack under mechanical stress, thereby releasing uncompensated charges, including those induced due to the direct piezoelectric effect, toward surface layers.

The oxidation state of both metals in PZO was identified with the X-ray absorption near edge structure (XANES) spectra of PZO and PZO320, collected at the Zr K-edge (Figure 5a) and Pb L_3 -edge (Figure 5b). They are reported in Figure 4 together with reference compounds, ZrO_2 and PbO , for the sake of comparison. The measured spectra demonstrate very few differences in the near-edge spectral region, which may be indicative of slight variations in the local environment of Zr and Pb sites. The analysis of spectral profiles led to the conclusion that Zr and Pb are in the oxidation state of 4+ and 2+, respectively. A poor signal-to-noise ratio in the extended X-ray absorption fine structure (EXAFS) spectra did not allow performing a more quantitative analysis of the potential differences.

The measured dielectric properties of PZO and PZO160 are reported in Figure 6. The AFE–FE phase transition is smoothed and accompanied by the relaxor behavior of both real (ϵ') and imaginary (ϵ'') parts of the dielectric constant, ϵ . The interval of existence of the intermediate phase was estimated using the $\epsilon(T)$ curve measured at 10 Hz. It is located between the 195 and 228 °C, and depends on the activation pressure.

The high-temperature FE–PE phase transition is the first-order process. The permittivity exhibits a finite maximum at T_C , where the two phases are in equilibrium. The Curie–Weiss temperature, T_{CW} , was determined from linear regression fits of the inverse permittivity versus temperature 1 kHz curve for PZO and PZO160. The curves demonstrate linear intervals above T_C , the Curie–Weiss law is obeyed within ≈ 6 °C for PZO, and the interval extends up to 10 °C for PZO160. Accordingly, the estimated values of the Curie–Weiss constant, C , were 5.9×10^4 and 4.5×10^4 °C. The

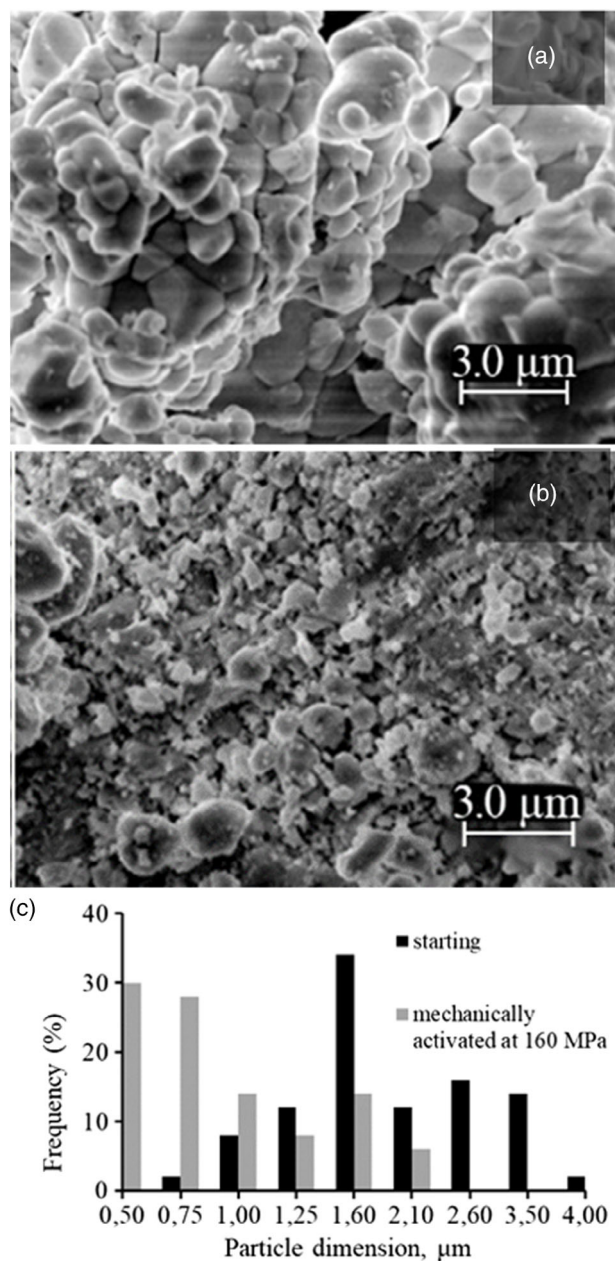


Figure 4. Electron micrographs of a) PZO and b) PZO160, and c) the particle size distribution histograms.

existence interval of the intermediate phase in PZO160 is assumed to be larger due to a substantial decrease in the AFE–FE transition temperature. There is a slight decrease in T_C too.

The Curie–Weiss constant goes down with increasing activation pressure. Instead, the ϵ_m values corresponding to T_C were larger for PZO160 than for PZO (Figure 6). This is because the structural defects, which have been accumulating in crystallites under stress, have not completely “dissolved” during the subsequent sintering of ceramics. Instead, they have contributed to the formation of pores, whose presence accounts for the high dielectric constant of the ceramics.

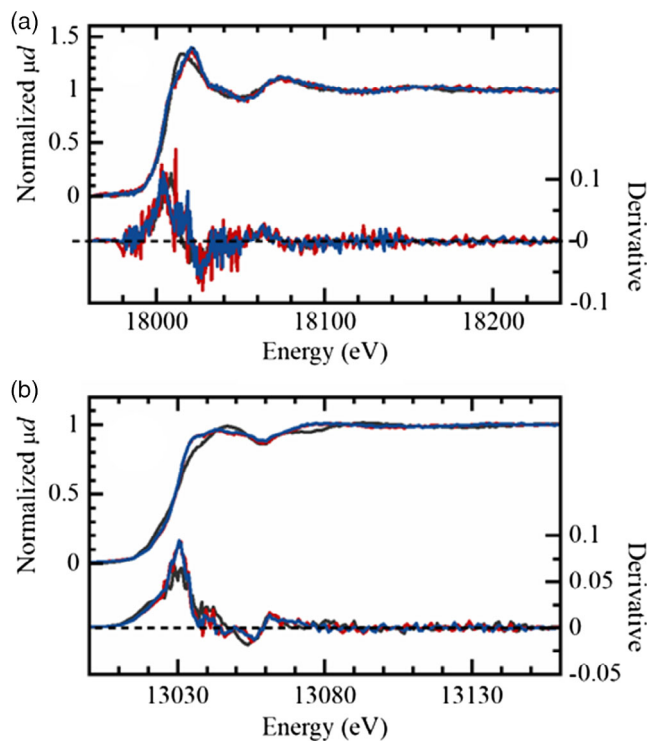


Figure 5. a) Zr *K*-edge and b) Pb *L*₃-edge XANES spectra of PZO (blue) and PZO320 (red), and the reference oxides, PbO and ZrO₂ (black).

The bandgap between the valence and conduction bands, E_g , is one of the most important parameters of perovskites. It is sensitive to structural perfection and the crystallite size, and can be found from the intrinsic optical properties. The analysis of the absorption edge allows establishing the type of optical transition and its anomalies, if any. Previously, $E_g = 3.4$ eV was reported for

PbZrO₃.^[31] However, other authors announced values of up to 3.930 eV,^[32] evidencing that E_g depends on the quality of the material and the measurement method.

The optical spectra of PZO and PZO160 are reported in **Figure 7** in Kubelka–Munk function values, $F(R_\infty)$, which are proportional to the absorption coefficient, α (see Equation (S4), Supporting Information). We adopted a Tauc plot method (see Equation (S5), Supporting Information) to find E_g . Assuming the direct transitions in PZO, we plotted the $(E \cdot F(R))^2$ versus $h\nu$ dependency (see Equation (S6), Supporting Information) from the measured spectra. The intersection point of the tangent to the straight section of the experimental curve with the abscissa axis graphically determines the E_g value. The obtained values are reported in Table 1.

The absorption of optical radiation with the energy below E_g appears in a spectral profile as the Urbach tail.^[33] Generally, there should be no absorption of quanta with energy below E_g in material with direct transitions (see Equation (S6), Supporting Information). This is reflected by the sharp edge of fundamental absorption from a lower energy side. Finding a linear interval within the $(F(E) \cdot E)^{1/n}$ curve is rather difficult when some transitions exist in proximity of E_g . If the compound of interest has an amorphous or strongly disordered structure, then transitions occurring between the localized states and corresponding to the Urbach tail absorb at $E \leq E_g$, hence leading to a nonlinear behavior of $(F(E) \cdot E)^{1/n}$ for energies $E \sim E_g$. The inset in **Figure 7** shows a zoomed interval of low-energy phonons, where the Urbach tail appears. The local energy levels, E_i , calculated from the absorption spectra of the initial and activated samples (for the AFE phase) are given in Table 1.

Another explanation for the observed experimental patterns at energies smaller than the bandgap is based on the concept of a random field of electric fluctuations. When the lattice vibrations are nonzero, fluctuations in the free charge carrier density initiate the appearance of random electric fields. The latter phenomena in a crystal are reflected by a long-wavelength tail in the

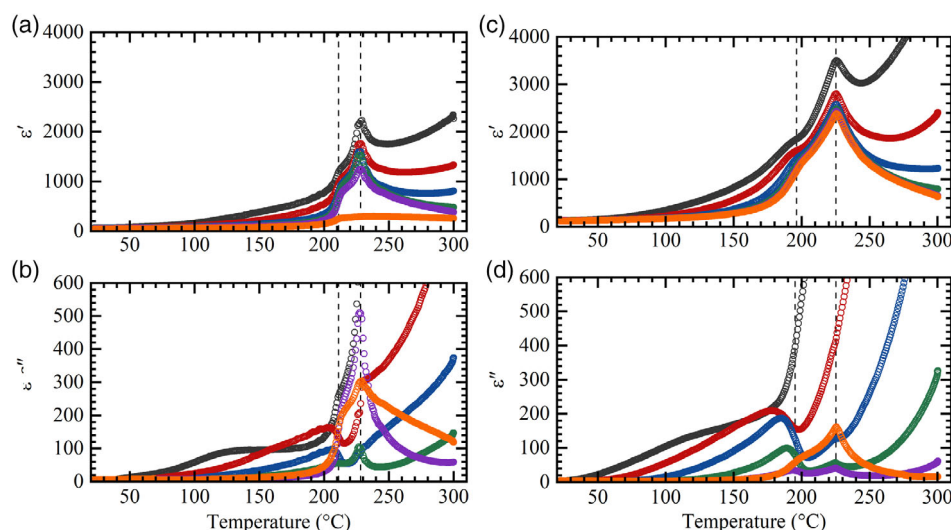


Figure 6. Temperature dependencies of the a,c) real and b,d) imaginary parts of the dielectric constant of PZO (a,b) and PZO160 (c,d). Frequencies of 10, 100 Hz, 1 kHz, 10, 100 kHz, and 1 MHz are shown by black, red, blue, green, purple, and orange colors, respectively. Vertical dashed lines highlight the characteristic features. Note: (c) the purple curve lies behind the orange one.

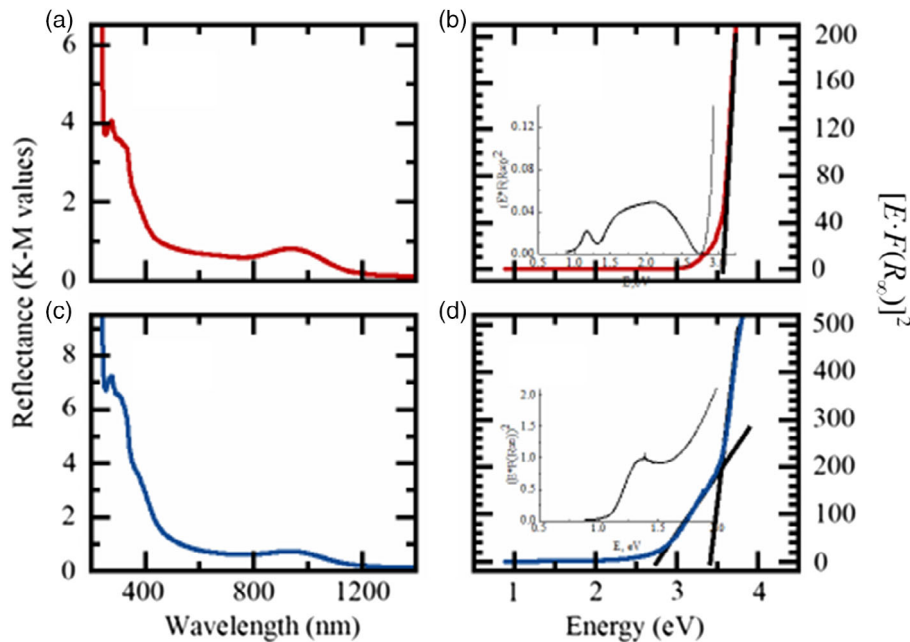


Figure 7. a,c) UV-vis spectra of a,b) PZO and b,d) PZO160 ceramics, and the correspondent Tauc plots (b,d). The insets in (b,d) show a zoomed interval for the Urbach tail absorption.

optical absorption curve. In the semiclassical approximation, the presence of a Gaussian random field is taken into account by an exponential expression for the spectral dependency of the absorption coefficient in the Urbach tail region.^[34]

As shown in the insets in Figure 7, PZO and PZO160 have different absorption profiles in the Urbach tail region, most likely caused by chemical and structural inhomogeneities in PZO (the inset in Figure 7b). During mechanical activation, the effective diffusion coefficient significantly increases, whereas the activation energy of diffusion processes decreases. These are favorable presettings for the subsequent thermal annealing (sintering of powder into ceramics), which facilitates the structural homogenization and forces eventual impurities to migrate toward the surface of crystallites and then be released into the atmosphere. Probably because of this, the Urbach tail in PZO160 has a less complex shape (the inset in Figure 7d).

3. Conclusion

We have characterized the properties of PbZrO_3 in the form of powder and ceramics after applying a quasi-hydrostatic mechanical load in combination with shear deformation in the 40–320 MPa pressure range. Such mechanical stress has led to the formation of multiscale particles saturated with structural defects in concentration proportional to the applied pressure. The particles are assumed to reside in various metastable states. The stress-induced impact on PZO was assessed from changes in such structural parameters such as the dimension of the unit cell, the size of the coherent scattering region, and microstrains. The dynamic properties of the crystal lattice after mechanical activation were studied in the Debye approximation by calculating the Debye

characteristic temperature and the isotropic Debye–Waller factor. All the monitored parameters demonstrate a nonmonotonous dependency in response to the applied pressure. It was also found that mechanical activation changes the optical absorption profile in the low-energy phonon region, which has been analyzed according to the Urbach tail approach.

4. Experimental Section

PZO ceramics were synthesized by the solid state reaction method.^[22] Briefly, chemically pure PbO and ZrO_2 were taken in a stoichiometric ratio and mixed well with the addition of ethanol in an agate mortar and pestle for 2 h. The mixture was compacted into tablets and sintered at 1200 °C (± 1 °C) for 2 h in an air atmosphere in closed crucibles amid PbZrO_3 powder to restore the escaping lead oxide. The products were ground into powder for the measurements and mechanoactivation.

For mechanoactivation, the PZO powder was divided into portions of equal weight and subjected to compression in Bridgman anvil pressure cells.^[23c] Pressures from 40 to 320 MPa were applied for 40 min. During this time the lower anvil completed two circular turns (720 angular degrees). The compacts were sintered at 1150 °C for 2 h at once with the PZO powder for backfill. The density of the resulting ceramics was 8 g cm^{-3} . Samples were labeled as “PZO” for the pristine PbZrO_3 , while the rest were indexed according to the applied pressure, e.g., “PZO160” for 160 MPa.

The XRD patterns were collected on a Bruker D2 PHASER diffractometer, which uses $\text{Cu K}\alpha$ radiation, with the 2θ step of 0.01° and the acquisition time of 0.1 s per point. Atomic positions and the isotropic temperature factor were varied in the Powder CELL 2.3 code for the Rietveld refinement.^[35] The R -factor was in the range of 7–9%. The JSCD database was consulted for the crystalline phase identification. For the two-temperature method, the integral intensities of the (110) and (220) reflections, $I_{(110)}$ and $I_{(220)}$, were measured at 773 and 873 K using a high-temperature homemade accessory for the diffractometer.^[22] The plotted values were graphically connected with B-spline lines.

The microscopic imaging was performed on a Carl Zeiss EVO 40 scanning electron microscope (SEM) operating at EHT (extra high tension) of 20 kV and I_{probe} of 50 pA.

The Pb L_3 -edge and Zr K -edge X-ray absorption spectra (XAS) were measured on a Rigaku R-XAS Looper laboratory spectrometer. An ionization chamber filled with Ar (300 mbar) was used to measure the X-ray beam intensity before the sample, and a scintillation detector was measuring the intensity after the sample. Ge (440), giving an energy resolution of $\Delta E = 3.1$ eV at the Pb L_3 -edge (13 035 eV), and Ge (840), providing $\Delta E = 3.5$ eV at the Zr K -edge (17 998 eV), were used for monochromatization of the beam. For each sample, six XANES spectra were acquired and averaged.

The dielectric properties were analyzed with an E7-20 automatic impedance meter manufactured by the Minsk R&D Institute of Instrument Making (Belarus). A firing-type silver conductive paste was utilized to cast electrodes on ceramic discs.

The optical spectra were recorded at room temperature in reflectance mode with 2 nm step acquisition on a Shimadzu UV-2600 spectrophotometer equipped with an integrating sphere accessory. The reflectance values (%R against BaSO₄ blank) were converted into Kubelka–Munk function using the instrument's software UVProbe.

Samples were measured in the form of powder except for the dielectric and optical measurements. For the two latter cases, discs with a diameter of 10 mm and a thickness of ≈ 1 mm were made using a conventional hydraulic powder compacting press.

Supporting Information

Supporting Information is available from the Wiley Online Library or from the author.

Acknowledgements

SEM imaging was conducted at the SSC RAS Center of Collective Use (No. 501994). The work was conducted within the State assignment of SSC RAS (project No. AAAA-A19-119040390084-3). A.P. acknowledges President's grant MK-5853.2021.1 for funding XAS measurements and analysis. XAS and UV–Vis data were collected at the Center of Collective Use Nanoscale Structure of Materials.

Conflict of Interest

The authors declare no conflict of interest.

Data Availability Statement

Research data are not shared.

Keywords

dielectric properties, lead zirconate, mechanoactivation, optical spectra, structural defects

Received: December 9, 2020

Revised: May 18, 2021

Published online: June 25, 2021

[1] H. Liu, B. Dkhlil, Z. Kristallogr. **2011**, 226, 163.

[2] a) C. Kittel, *Phys. Rev.* **1951**, 82, 729; b) G. Shirane, E. Sawaguchi, Y. Takagi, *Phys. Rev.* **1951**, 84, 476; c) E. Sawaguchi, H. Maniwa, S. Hoshino, *Phys. Rev.* **1951**, 83, 1078.

[3] X. Hao, J. Zhai, L. B. Kong, Z. Xu, *Prog. Mater. Sci.* **2014**, 63, 1.

[4] a) M. A. Pena, J. L. G. Fierro, *Chem. Rev.* **2001**, 101, 1981; b) C. Sun, J. A. Alonso, J. Bian, *Adv. Energy Mater.* **2020**, 11, 2000459.

[5] a) M. Kimura, A. Ando, D. Maurya, S. Priya, in *Advanced Piezoelectric Materials*, 2nd ed., (Ed: K. Uchino), Woodhead Publishing, Duxford, **2017**, pp. 95–126; b) Z. Liu, T. Lu, J. Ye, G. Wang, X. Dong, R. Withers, Y. Liu, *Adv. Mater. Technol.* **2018**, 3, 1800111.

[6] H.-J. Lee, S.-S. Won, K.-H. Cho, C.-K. Han, N. Mostovych, A. I. Kingon, S.-H. Kim, H.-Y. Lee, *Appl. Phys. Lett.* **2018**, 112, 092901.

[7] M. Glazer, K. Roleder, J. Dec, *Acta Cryst.* **1993**, B49, 846.

[8] S. Roberts, *J. Am. Ceram. Soc.* **1950**, 33, 63.

[9] A. Tagantsev, K. Vaideeswaran, S. Vakhrushev, A. Filimonov, R. Burkovsky, A. Shaganov, D. Andronikova, A. Rudskoy, A. Baron, H. Uchiyama, D. Chernyshov, A. Bosak, Z. Ujma, K. Roleder, A. Majchrowski, J.-H. Ko, N. Setter, *Nat. Commun.* **2013**, 4, 2229.

[10] R. G. Burkovsky, I. Bronwald, D. Andronikova, B. Wehinger, M. Krisch, J. Jacobs, D. Gambetti, K. Roleder, A. Majchrowski, A. V. Filimonov, A. I. Rudskoy, S. B. Vakhrushev, A. K. Tagantsev, *Sci. Rep.* **2017**, 7, 41512.

[11] a) Z. Xu, X. Dai, D. Viehland, D. A. Payne, *J. Am. Ceram. Soc.* **1995**, 78, 2220; b) J.-H. Ko, M. Gorny, A. Majchrowski, K. Roleder, A. Bussmann-Holder, *Phys. Rev. B* **2013**, 87, 184110.

[12] X. Dai, J.-F. Li, D. Viehland, *Phys. Rev. B* **1995**, 51, 2651.

[13] a) E. Sawaguchi, G. Shirane, Y. Takagi, *J. Phys. Soc. Jpn.* **1951**, 6, 333; b) V. J. Tennery, *J. Electrochem. Soc.* **1965**, 112, 1117; c) X. Dai, Z. Xu, D. Viehland, *J. Appl. Phys.* **1995**, 77, 5086.

[14] L. Benguigui, *J. Solid State Chem.* **1971**, 3, 381.

[15] B. A. Scott, G. Burns, *J. Am. Ceram. Soc.* **1972**, 55, 331.

[16] H. Liu, *J. Am. Ceram. Soc.* **2018**, 101, 5281.

[17] J. Dec, J. Kwapulinski, *J. Phys.: Condens. Matter* **1989**, 1, 3389.

[18] V. V. Prisedsky, V. P. Komarov, G. F. Panko, V. V. Klimov, *Ferroelectrics* **1980**, 23, 23.

[19] A. Pramanick, A. D. Prewitt, J. S. Forrester, J. L. Jones, *Crit. Rev. Solid State*, **2012**, 37, 243.

[20] M. A. Sirota, K. G. Abdulvakhidov, *J. Surf. Invest.: X-Ray, Synchrotron Neutron Technol.* **2017**, 11, 677.

[21] K. G. Abdulvakhidov, M. A. Sirota, A. P. Budnyk, T. A. Lastovina, A. V. Soldatov, S. N. Kallayev, Z. M. Omarov, S. A. Sadykov, B. K. Abdulvakhidov, M. A. Vitchenko, I. V. Mardasova, P. S. Plyaka, R. G. Mitarov, *Mater. Res. Express* **2018**, 5, 115029.

[22] K. G. Abdulvakhidov, M. A. Sirota, A. P. Budnyk, T. A. Lastovina, B. K. Abdulvakhidov, S. A. Sadykov, P. S. Plyaka, A. V. Soldatov, *J. Phys.: Condens. Matter* **2019**, 31, 135402.

[23] a) K. G. Abdulvakhidov, E. N. Ubushaeva, I. V. Mardasova, M. A. Vitchenko, B. K. Abdulvakhidov, V. G. Zaletov, A. A. Amirov, I. K. Kamilov, A. S. Manukyan, P. S. Plyaka, G. B. Sukharina, *Ferroelectrics* **2016**, 494, 182; b) K. G. Abdulvakhidov, S. N. Kallaev, M. A. Kazaryan, P. S. Plyaka, S. A. Sadikov, M. A. Sirota, S. V. Zubkov, *Mater. Sci. Eng.* **2016**, 112, 1; c) M. A. Sirota, K. G. Abdulvakhidov, A. P. Budnyk, A. V. Soldatov, A. L. Bugaev, T. A. Lastovina, Yu. V. Kabirov, M. I. Mazuritskiy, P. S. Plyaka, S. N. Kallaev, Z. M. Omarov, S. A. Sadykov, B. K. Abdulvakhidov, I. V. Mardasova, M. A. Vitchenko, *Ferroelectrics* **2018**, 526, 1.

[24] M.A. Krivoglaз, *Theory of X-Ray and Thermal Neutron Scattering by Real Crystals*, Springer, Berlin **1969**.

[25] A. Maradudin, *The Defects and the Vibrational Spectrum of Crystals*, Mir, Moscow, **1968**.

[26] H. Fujishita, Y. Shiozaki, N. Achiwa, E. Sawaguchi, *J. Phys. Soc. Japan* **1982**, 51, 3583.

[27] A. M. Glazer, *Acta Cryst. B* **1993**, 49, 846.

[28] K. Wiczorek, A. Ziebiniska, Z. Ujma, K. Szot, M. Gorny, I. Franke, J. Koperski, A. Soszyński, K. Roleder, *Ferroelectrics* **2006**, 336, 61.

[29] Y. S. Umanski, *X-Ray Investigation of Metals and Semiconductors*, Metallurgia, Moscow, **1969**.

- [30] R. W. James, *The Optical Principles of the Diffraction of X-Rays*, G. Bell and Sons, London, **1950**.
- [31] M. P. Moret, M. A. C. Devillers, K. Wörhoff, P. K. Larsen, *J. Appl. Phys.* **2002**, 92, 468.
- [32] V. I. Zaimin, *Phys. Status Solidi B* **1984**, 124, 625.
- [33] F. Urbach, *Phys. Rev.* **1953**, 92, 1324.
- [34] V. L. Bonch-Bruевич, *Phys. Status Solidi* **1970**, 42, 35.
- [35] W. Kraus, G. Nolze, *J. Appl. Cryst.* **1996**, 29, 301.